

SCALING UP AND STABILIZING DIFFERENTIABLE PLANNING WITH IMPLICIT DIFFERENTIATION

Lin Feng Zhao^{1*}, Huazhe Xu², Lawson L.S. Wong¹

¹Khoury Colleges of Computer Science, Northeastern University,

²Institute for Interdisciplinary Information Sciences, Tsinghua University,

³Shanghai Qi Zhi Institute

ABSTRACT

Differentiable planning promises end-to-end differentiability and adaptivity. However, an issue prevents it from scaling up to larger-scale problems: they need to differentiate through forward iteration layers to compute gradients, which couples forward computation and backpropagation and needs to balance forward planner performance and computational cost of the backward pass. To alleviate this issue, we propose to differentiate through the Bellman fixed-point equation to decouple forward and backward passes for Value Iteration Network and its variants, which enables constant backward cost (in planning horizon) and flexible forward budget and helps scale up to large tasks. We study the convergence stability, scalability, and efficiency of the proposed implicit version of VIN and its variants and demonstrate their superiorities on a range of planning tasks: 2D navigation, visual navigation, and 2-DOF manipulation in configuration space and workspace.

1 INTRODUCTION

Planning is a crucial ability in artificial intelligence and robotics (LaValle, 2006; Sutton & Barto, 2018). Typically, a planning algorithm either uses a ground-truth dynamics model or takes as input a separately learned model. It enables jointly learning a compact MDP that promises the learned value is equivalent to the original problem. Recently, *differentiable planning* (Tamar et al., 2016; Schrittwieser et al., 2019; Oh et al., 2017; Grimm et al., 2020; 2021) alleviates these requirements by training models and policies in an end-to-end manner. It enables jointly learning a compact MDP and promises that the learned value is equivalent to the original problem.

However, current differentiable planning suffers from scalability and convergence stability issues because it requires to differentiate through the planning computation. When performing the differentiation, we inevitably need to iteratively unroll network layers to improve value estimates, especially for long-horizon planning problems. It results in slower inference and, more fatally, inefficient and unstable gradient computation through multiple network layers. Thus, this work aims to study the question: *can we scale up differentiation planning and keep the training efficient and stable?*

We find the bottleneck is caused by *explicit differentiation*, which backpropagates gradients through layers and thus couples forward and backward passes. Instead, since the Bellman equations define a fixed-point system, the solution is defined by an implicit function and can be solved with *implicit differentiation*. Value Iteration Networks (VINs) (Tamar et al., 2016) use convolution networks to solve the fixed-point problem by embedding value iteration into its computation. We propose to use implicit differentiation for VIN-based planners to compute the equilibrium, including Gated Path Planning Networks (GPPN) (Lee et al., 2018) and Symmetric VIN (SymVIN) (Zhao et al., 2022), and name it *implicit differentiable planning (IDP)*. This implicit differentiation idea has also been recently studied in supervised learning (Bai et al., 2019; Winston & Kolter, 2021; Amos & Yarats, 2019; Amos & Kolter, 2019).

Using implicit differentiation in planning brings several benefits. It decouples forward and backward passes, so when the forward pass scales up to more iterations for long-horizon planning problems,

*Corresponding Author: Lin Feng Zhao zhao.lin@northeastern.edu.

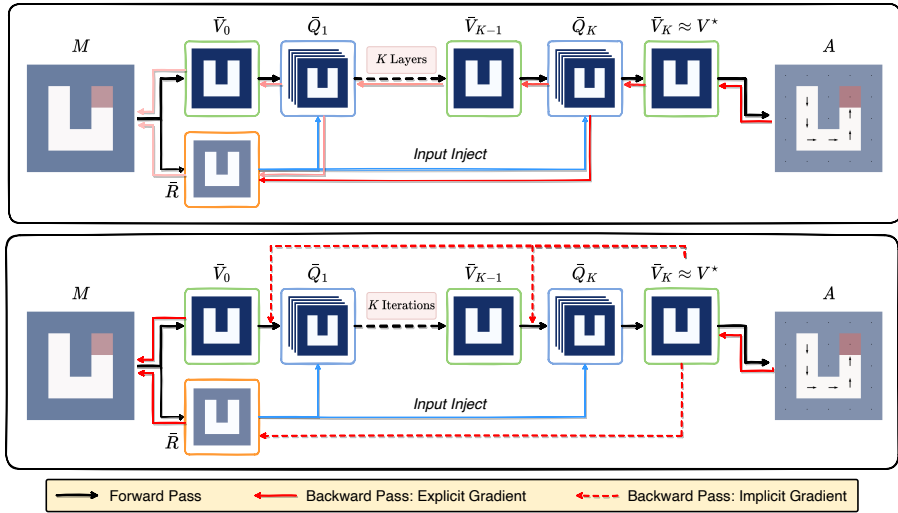


Figure 1: An overview of VIN, a differentiable planner with explicit differentiation, and ID-VIN, our proposed planner with implicit differentiation. Lighter colors for the backward pass with explicit differentiation (solid red arrows) indicate larger backpropagation depth. For backward passes with implicit differentiation, the dashed red arrows start from the solved equilibrium V^* and end at each forward layer (black arrows).

the backward pass can stay constant cost. It is also no longer constrained to differentiable forward solvers/planners, potentially allowing other non-differentiable operations in planning. It can potentially reuse intermediate computation from forward computation in the backward pass, which is infeasible for explicit differentiation. We focus on scaling up implicit differentiable planning to larger planning problems and stabilizing its convergence, and also experiment with different optimization techniques and setups. In our experiments on various tasks, the planners with implicit differentiation can train on larger tasks, plan with a longer horizon, use less (backward) time in training, converge more stably, and exhibit better performance compared to explicit counterparts. We summarize our contributions below:

- We apply implicit differentiation on VIN-based differentiable planning algorithms. This connects with deep equilibrium models (DEQ) (Bai et al., 2019) and prior work in both sides, including (Bai et al., 2021; Nikishin et al., 2021; Gehring et al., 2021).
- We propose a practical implicit planning pipeline and implement implicit version of VIN, as well as GPPN (Lee et al., 2018) and SymVIN (Zhao et al., 2022).
- We empirically study the convergence stability, scalability, and efficiency of the explicit planners and proposed implicit planners, on four planning tasks: 2D navigation, visual navigation, and 2 degrees of freedom (2-DOF) manipulation in configuration space and workspace.

2 RELATED WORK

Differentiable Planning In this paper, we use *differentiable planning* to refer to planning with neural networks, which can also be named *learning to plan* and may be viewed as a subclass of *integrating planning and learning* (Sutton & Barto, 2018). It is promising because it can be integrated into a larger differentiable system to form a closed loop., Grimm et al. (2020; 2021) propose to understand model-based planning algorithms from value equivalence perspective. Value iteration network (VIN) (Tamar et al., 2016) is a representative work that performs value iteration using convolution on lattice grids, and has been further extended (Niu et al., 2017; Lee et al., 2018; Chaplot et al., 2021; Deac et al., 2021). Other than using convolution network, the work on integrating learning and planning into differentiable networks includes (Oh et al., 2017; Karkus et al., 2017; Weber et al., 2018; Srinivas et al., 2018; Schrittwieser et al., 2019; Amos & Yarats, 2019; Wang & Ba, 2019; Guez et al., 2019; Hafner et al., 2020; Pong et al., 2018; Clavera et al., 2020).

Implicit Differentiation Beyond computing gradients by following the forward pass layer-by-layer, the gradients can also be computed with *implicit differentiation* to bypass differentiating

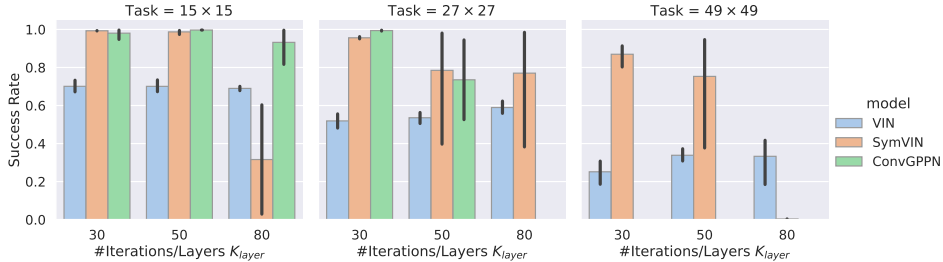


Figure 2: Demonstration of differentiable planners with explicit differentiation, which cannot scale up to large tasks or more iterations, due to coupled forward and backward pass.

through some advanced root-find solvers. This strategy has been used in a body of recent work (Chen et al., 2019; Bai et al., 2019; Amos & Kolter, 2019; Ghaoui et al., 2020). Particularly related, Bai et al. (2019) propose *Deep Equilibrium Models (DEQ)* that decouples the forward and backward pass and solve the backward pass iteratively also through a fixed-point system. Winston & Kolter (2021) study the convergence of fixed point iteration in a specific type of deep network. Amos & Kolter (2019) formalize optimization as a layer, and Amos & Yarats (2019) further apply the idea to iterative LQR. Gehring et al. (2021) theoretically study gradient dynamics of implicit parameterization of value function through the Bellman equation. Nikishin et al. (2021) similarly use implicit differentiation, while they explicitly solve the backward pass and only work on small-scale tasks because explicit solving is not scalable. Bacon et al. (2019) instead focus on a Lagrangian perspective. Our work is focused on scalability and convergence stability on differentiable planning, and experiments with challenging tasks in simulation to empirically justify the approach.

3 DIFFERENTIABLE PLANNING WITH EXPLICIT DIFFERENTIATION

Background: Value Iteration Networks. Value iteration is an instance of the dynamic programming (DP) method to solve Markov decision processes (MDPs). It iteratively applies the Bellman (optimality) operator until convergence, which is based on the following Bellman (optimality) equation: $Q(s, a) = R(s, a) + \gamma \sum_{s'} P(s'|s, a)V(s')$ and $V(s) = \max_a Q(s, a)$.

Tamar et al. (2016) used a convolution network to parameterize value iteration, named Value Iteration Network (VIN). VINs jointly learn and plan in a latent MDP on the 2D grid, which has the latent reward function $\bar{R} : \mathbb{Z}^2 \rightarrow \mathbb{R}^{|\mathcal{A}|}$ and has transition probability \bar{P} represented as $W^V : \mathbb{Z}^2 \rightarrow \mathbb{R}^{|\mathcal{A}|}$, which only relies on differences between states. The value function is written as $\bar{V} : \mathbb{Z}^2 \rightarrow \mathbb{R}$ and $\bar{Q} : \mathbb{Z}^2 \rightarrow \mathbb{R}^{|\mathcal{A}|}$. Value iteration can be written as:

$$\bar{Q}_{\bar{a}, i', j'}^{(k)} = \bar{R}_{\bar{a}, i, j} + \sum_{i, j} W_{\bar{a}, i, j}^V \bar{V}_{i' - i, j' - j}^{(k-1)}, \quad \bar{V}_{i, j}^{(k)} = \max_{\bar{a}} \bar{Q}_{\bar{a}, i', j'}^{(k)}. \tag{1}$$

If we let \mathbf{f} be a single application of the Bellman operator, Eq. 1 can be written as:

$$\bar{V}^{(k)} = \mathbf{f}(\bar{V}^{(k-1)}, \bar{R}, W^V) \equiv \max_{\bar{a}} \bar{R}^{\bar{a}} + W_{\bar{a}}^V \star \bar{V}^{(k-1)} \equiv \max_{\bar{a}} \bar{R}^{\bar{a}} + \text{CONV2D}(\bar{V}^{(k-1)}; W_{\bar{a}}^V) \tag{2}$$

where convolution $W_{\bar{a}}^V \star V$ is implemented as a 2D convolution layer CONV2D with learnable weight W^V . For simplicity, we later use θ to refer to network weights, and write each iteration as $\mathbf{v}_{k+1} = \mathbf{f}(\mathbf{v}_k, \mathbf{r}, \theta)$, where \mathbf{r} stands for reward map \bar{R} and \mathbf{v}_k for value map $\bar{V}^{(k)}$.

Pitfall: Coupled forward and backward pass. The forward computation of VIN iteratively applies the Bellman update \mathbf{f} . Thus, the optimization needs automatic differentiation: differentiating through multiple layers of forward iterations $\mathbf{f} \circ \mathbf{f} \circ \dots \circ \mathbf{f}$. Using automatic differentiation for VIN has a major drawback: the forward computation of value iteration (“forward pass”) and the computation of its gradients (“backward pass”) are *coupled*. That is, if the planning horizon is enlarged, VINs would need larger number of iterations to propagate the value from goals to remaining positions. As used in VIN and GPPN (Tamar et al., 2016; Lee et al., 2018), it requires intensive memory usage to store every intermediate iterate $V^{(k)}$ to enable automatic differentiation.

To illustrate the effects, we show the performance of *explicit planners* in Figure 2, including three models with increasingly higher memory use and time cost: VIN, SymVIN (Zhao et al., 2022) and

ConvGPPN (a modified version of GPPN (Lee et al., 2018)). They are trained on 15×15 , 27×27 , and 49×49 path planning tasks. To solve larger mazes, each model consumes more memory while also needing more iterations (x-axes). However, since explicit differentiation requires backpropagating gradients layer by layer, with more iterations or larger tasks, some models either diverge or run out of memory (11GB limit). We present further experimental details and analyses in Section 5.2.

4 APPROACH: FROM *Explicit* TO *Implicit Differentiation* FOR PLANNING

This section introduces a strategy with *implicit differentiation* to resolve the issue by decoupling the forward and backward computation. We first derive implicit differentiation for VIN-based planners, then propose a pipeline for implementing those planners with implicit differentiation. We refer to them as *implicit planners*, in contrast to *explicit planners* with explicit differentiation. We analyze the technical differences and similarities of implicit planners vs. explicit planners afterward.

4.1 IMPLICIT DIFFERENTIATION FOR VALUE ITERATION

We derive implicit differentiation for VIN and variants, where each layer f is a step as in value iteration. Since the derivation does not rely on the concrete instantiation of f , we can freely replace f from `Conv2D` with other types of layers. We will introduce these variants in the next subsection.

Implicit differentiation. A fixed-point problem can be solved iteratively by fixed-point iteration and other algorithms. However, as pointed out in (Bai et al., 2019), naively differentiating through the solver would require intensive memory usage, since it needs to store every intermediate iterate $V^{(k)}$ to enable automatic differentiation, as in (Tamar et al., 2016; Lee et al., 2018). As also used recently in (Bai et al., 2019; Nikishin et al., 2021; Gehring et al., 2021), another solution is to instead differentiate directly through the fixed point z^* using the implicit function theorem and implicit differentiation. Then, we can skip all of this by decoupling forward (fixed-point iteration as the solver) and backward pass (differentiating through the solver).

We start with the fixed point equation $v^* = f(v^*, r, \theta)$ from the Bellman optimality equation. Below we use x to stand for either input r or θ . The implicit function theorem tells us that, under some mild conditions of the derivatives (f is continuously differentiable with non-singular Jacobian $\partial f(v, x)/\partial x$), $v^*(x)$ is a differentiable function of x locally: $0 = f(v^*(x), x)$.

For fixed point equation, we can assume the fixed point solution v^* is obtained, thus this can be used to compute the partial derivative w.r.t. to any quantity (input, parameter, etc) $\partial v^*(\cdot)/\partial(\cdot)$. It avoids backpropagating gradients through the forward fixed-point iteration, which is computationally inefficient and requires considerable memory to store intermediate iteration variables. Additionally, it also allows to even use of non-differentiable operations in the forward pass.

Differentiating both sides of the equation $v^* = f(v^*, x)$ and applying the chain rule:

$$\frac{\partial v^*(\cdot)}{\partial(\cdot)} = \frac{\partial f(v^*(\cdot), x)}{\partial(\cdot)} = \frac{\partial f(v^*, x)}{\partial v^*} \frac{v^*(\cdot)}{\partial(\cdot)} + \frac{\partial f(v^*, x)}{\partial(\cdot)}, \quad (3)$$

where we use (\cdot) to denote an arbitrary variable. Rearranging terms:

$$\frac{\partial v^*(\cdot)}{\partial(\cdot)} = \left(I - \frac{\partial f(v^*, x)}{\partial v^*} \right)^{-1} \frac{\partial f(v^*, x)}{\partial(\cdot)}. \quad (4)$$

Solving backward pass. To integrate into a deep learning framework for automatic differentiation, two quantities are needed: VJP (vector-Jacobian product) and JVP (Jacobian-vector product) (Gilbert, 1992). Nevertheless, the computation of the inverse term $(I - \partial f(v^*, x)/\partial v^*)^{-1}$ can be a major bottleneck due to its dimension ($O(d^2)$ or $O(m^4)$, where $d = m^2$ is the matrix width and m is the map size) (Bai et al., 2019; 2021). Additionally, when applied to VINs, we concatenate a policy layer that maps the final equilibrium $v^* \in \mathbb{R}^{m \times m}$ to action logits $\mathbb{R}^{m \times m}$ and compute the cross-entropy loss $\ell(\cdot)$ (Tamar et al., 2016). Thus, the derivative of loss is:

$$\frac{\partial \ell}{\partial(\cdot)} = \frac{\partial \ell}{\partial v^*} \frac{\partial v^*(\cdot)}{\partial(\cdot)} = \frac{\partial \ell}{\partial v^*} \left(I - \frac{\partial f(v^*, x)}{\partial v^*} \right)^{-1} \frac{\partial f(v^*, x)}{\partial(\cdot)}, \quad (5)$$

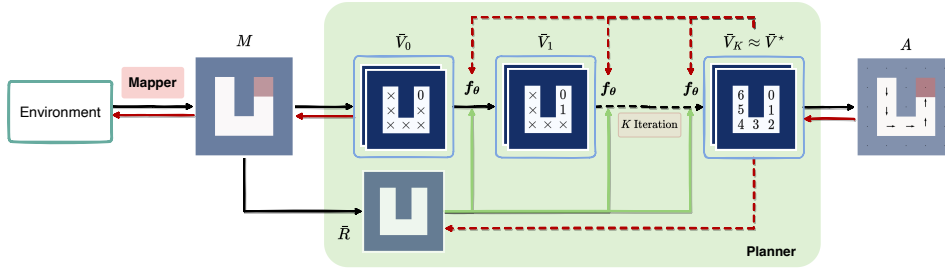


Figure 3: The proposed pipeline of implicit planning by using implicit differentiation.

Defining w as follows forms a linear fixed-point system (Bai et al., 2019):

$$w^\top \triangleq \frac{\partial \ell}{\partial v^*} \left(I - \frac{\partial f(v^*, x)}{\partial v^*} \right)^{-1}; \quad w^\top = w^\top \frac{\partial f(v^*, x)}{\partial v^*} + \frac{\partial \ell}{\partial v^*}. \quad (6)$$

This backward pass fixed-point equation can also be solved by a generic fixed-point solver or root finder. Then, we can substitute the solution w back: $\partial \ell / \partial (\cdot) = w^\top \partial f(v^*, x) / \partial (\cdot)$. The computation is then purely based on VJP and JVP. In summary, an implicit planner needs to solve both the (nonlinear) *forward* fixed-point system and the (linear) *backward* fixed-point system, as in DEQ.

4.2 A PIPELINE OF IMPLICIT PLANNING

We can derive variants of VIN using implicit differentiation by abstracting out the implementation of value iteration layer. In this section, we propose a generic implicit planning pipeline to extend our approach to Gated Path Planning Networks (GPPN) (Lee et al., 2018) and Symmetric VIN (SymVIN) (Zhao et al., 2022). Spatial Planning Transformers (SPT) (Chaplot et al., 2021) also fits into the pipeline, but it performs less well, as discussed in Section C.

Figure 3 shows the general pipeline, where the network layer f_θ can be replaced by any single layer that is capable of iterating values. The pipeline follows VIN and GPPN, where for 2D path planning a map $\mathbb{Z}^2 \rightarrow \{0, 1\}$ is provided, and the planners’ output actions (their logits) for each position $\mathbb{Z}^2 \rightarrow \mathbb{R}^{|\mathcal{A}|}$. We also run on other tasks including *visual navigation*, 2-DOF configuration space manipulation, and 2-DOF workspace manipulation, where all these tasks can be represented as taking a form of map “signal” over grid \mathbb{Z}^2 , as previously been done (Zhao et al., 2022; Chaplot et al., 2021). We use four directions as actions for all tasks: $\mathcal{A} = (\text{north}, \text{west}, \text{south}, \text{east})$.

Planner instantiations. We now introduce the instantiations of implicit planners one by one. We focus on the value iteration part (omit map input and action output), and all planners follow the form $\bar{V}^{(k+1)} = f_\theta(\bar{V}^{(k)}, \bar{R})$ (bars omitted later). There are two design principles: (1) input inject (\bar{R} must be input, as input x) and (2) weight-tied (θ is shared across layers f), as also used in DEQ (Bai et al., 2019). Specifically, the purpose of input inject is that fixed-point solution \bar{V}^* does not depend on initialization $\bar{V}^{(0)}$, so we must pass information of the map through input inject (by \bar{R}).

(i) **ID-VIN** uses regular 2D translation-equivariant convolution layer, where $f(V, R) = \max_a R^a + \text{Conv2D}(V; \theta)$. (ii) **ID-SymVIN** aims to integrate symmetry into planning and uses equivariant $E(2)$ -steerable CNN (Weiler & Cesa, 2021). It has similar form to VIN and just replaces Conv2D with SteerableConv, thus the form is $f(V, R) = \max_a R^a + \text{SteerableConv}(V; \theta)$.

(iii) **ID-ConvGPPN** is based on our modified version of GPPN [Redacted for anonymous review], where we (1) use GRU since it has a single input with form $z' = \text{GRU}(z, x)$ and is easier to integrate into our current form, (2) replace all fully connected layers with convolution layers, and (3) inject R to every step. The result is that every layer is a ConvGRU, instead of LSTM in GPPN: $f(V, R) = \text{ConvGRU}(V, R; \theta)$. Note that the GPPN variants do not have max in each iteration anymore and directly take reward R to the recurrent cell (Lee et al., 2018).

Mapper Layer. We can handle tasks with more challenging input, such as *visual navigation* and *workspace manipulation* (Lee et al., 2018; Chaplot et al., 2021; Zhao et al., 2022), by learning an additional mapping network (*mapper*) to first map the input to a 2D map. Further details about environments and mapper implementation are deferred to Section 5.1 and Section C.

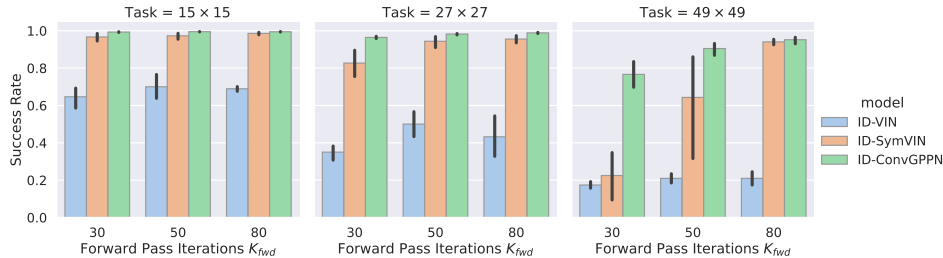


Figure 4: Performance of implicit planners on 2D navigation tasks. Since the forward and backward pass are decoupled, the implicit planners can keep consistent runtime and memory cost for backward pass while have forward pass of value iteration converged for large tasks and iterations.

Optimization. We adopt a body of work around deep equilibrium models (DEQ) (Bai et al., 2019; 2020; 2021), which adapts several empirically useful techniques. Since we have abstracted out the implementation of value iteration as fixed-point solving, we can use any fixed-point solver for $f(v, \theta) = v$ or root solver for $v - f(v, \theta) = 0$. As VIN does through its feedforward network (Tamar et al., 2016), a naïve solver is *forward iteration* $f(v_k, \theta) = v_{k+1}$. Additionally, recent work has been using Anderson’s method or Broyden’s method (Bai et al., 2019; 2020). We empirically compare using forward iteration or Anderson solver in forward and backward pass, separately. Note that SymVIN requires the entire forward pass to be equivariant, so the design of the forward solver needs extra care. We provide additional implementation details and results in Section C and E.

4.3 IMPLICIT VS. EXPLICIT DIFFERENTIABLE PLANNERS

Underlying computational similarity. The gradient computation is done by automatic differentiation (Gilbert, 1992). For *explicit differentiation*, the gradients are computed through direct backpropagation and the implementation is also based on efficiently computing vector-Jacobian product (VJP) and Jacobian-vector product (JVP) (Bai et al., 2019). Christianson (1994) studied automatic differentiation for implicit differentiation of fixed-point system. The only difference is the number of operations required and that implicit differentiation is based on the Jacobian at the equilibrium. We derive the connection in Section B.1.

Comparison: Implicit vs. explicit planners. Continuing on the empirical comparison, we show the performance of our three implicit planners with different iterations in forward pass in Figure 4. Compared to explicit planners in Figure 2, our implicit planners converge stably with larger (max) forward-pass iterations, while explicit planners sometimes diverge on large iterations.

Note that we should *not* directly compare implicit and explicit planners with the same numbers of forward iteration (horizontal axis), because they refer to different things: implicit planners rely on a reasonable equilibrium from forward pass to solve backward fixed-point equation (more forward iterations would be better), while for explicit planners # iterations = # layers (more iterations/layers leads to instability). We present further analyses in Section 5.2.

Tradeoff: The quality of equilibrium. Theoretically, implicit planners have a constant cost of the backward pass with respect to the forward planning horizon. However, the *backward pass* requires the Jacobian of the final equilibrium $v^* \approx v_K$ from the forward pass. If the equilibrium v^* is not solved reasonably well, the backward pass in Eq. 6 would iterate based on an inaccurate Jacobian $\partial f(v^*, x) / \partial v^*$, which would cause poor performance. In contrast, because explicit planners compute exact gradients by backpropagation through layers, they do not suffer from this issue. Additionally, fewer iterations (layers) would also alleviate their convergence issues.

Empirically, with fewer *forward iterations* (e.g., 10), we observed a performance drop from implicit planners. Although explicit planners also perform worse with fewer layers, they have a smaller drop compared to implicit planners. However, when scaling up to more forward iterations K_{fwd} (e.g. ≥ 30 iterations, which are necessary for maps $\geq 27 \times 27$) implicit planners may solve the equilibrium well enough and are more favorable because of their efficient backward pass. Moreover, we empirically found that using around $K_{bwd} \approx 15$ iterations for backward pass works well enough consistently across different map sizes (15×15 through 49×49). Since both explicit and implicit differentiation use a similar amount of vector-matrix products, using more than $K_{layer} \geq 15 \approx K_{bwd}$ would consume more resources and favor implicit planners.

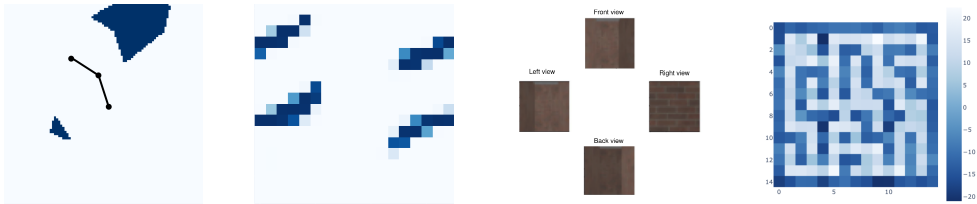


Figure 5: (1) **Workspace manipulation.** The top-down view is the *workspace* of a 2-DOF manipulation task. It is mapped by a mapper layer to configuration space, shown in subfigure (2), and provided to 2D planners as well. (3) **Visual navigation.** The environment provides a set of egocentric panoramic images for each location, where a set of panoramic images in four directions is visualized. Then, a mapper layer takes them as input and predicts a map, visualized in subfigure (4). The predicted map is used for 2D path planning.

5 EMPIRICAL ANALYSIS

We present more results on convergence, scalability, generalization, and efficiency on four different tasks, which extends the study in previous sections on comparing implicit vs. explicit planning.

5.1 ENVIRONMENTS AND SETUP

Environments and datasets. We run our implicit and explicit planners on four types of tasks: (1) **2D navigation**, (2) **visual navigation**, (3) 2 degrees of freedom (2-DOF) **configuration space manipulation**, and (4) **2-DOF workspace manipulation**. These tasks require planning on either *given* (2D navigation and 2-DOF configuration-space manipulation) or *learned* maps (visual navigation and 2-DOF workspace manipulation), where the maps are 2D regular grid as in prior work (Tamar et al., 2016; Lee et al., 2018; Chaplot et al., 2021). To learn maps, a planner needs to jointly learn a mapper that converts egocentric panoramic images (visual navigation) or workspace states (workspace manipulation) into a 2D grid. We follow the setup in (Lee et al., 2018; Chaplot et al., 2021) and further discuss in Section D. In both cases, we randomly generate training, validation and test data of $10K/2K/2K$ maps for all map sizes. For all maps, the action space is to move in 4 \odot directions: $\mathcal{A} = (\text{north, west, south, east})$.

Training and evaluation. We report success rate and training curves over 5 seeds. The training process (on given maps) follows (Tamar et al., 2016; Lee et al., 2018; Zhao et al., 2022), where we train 60 epochs with batch size 32, and use kernel size $F = 3$ by default. We use RTX 2080 Ti cards with 11GB memory for training, thus we use 11GB as the memory limit for all models.

5.2 CONVERGENCE AND SCALABILITY

In the previous sections with Figure 2 and 4, we have presented quantitative analysis of implicit and explicit planners in terms of convergence with more iterations and scalability on larger tasks. Here, we provide the detailed setup of the experiment and put the attention more on the qualitative side.

Setup. We train all models on 2D maze navigation tasks with map sizes 15×15 , 27×27 , and 49×49 . We use $K_{\text{layer}} = 30, 50, 80$ iterations for *explicit planners*, which is effectively the number of layers in their networks. Correspondingly, for *implicit planners*, we choose to use *forward iteration* solver for forward pass and Anderson solver for backward pass. We fix the number of iterations of backward solver as $K_{\text{bwd}} = 15$ and of forward solver as $K_{\text{fwd}} = 30, 50, 80$.

Results. We examine results by algorithm and focus on their trend with iteration number (x-axis) and map size (column), not just the absolute numbers. The conclusion already mentioned in the above section: Beyond an intermediate iteration number (around 30-50), implicit planners are more favorable because of scalability and computational cost. We present other analyses here.

We start from ConvGPPN and ID-ConvGPPN, which perform the best in explicit and implicit planner class, respectively. They also have the most number of parameters and use greatest time because of the gates in ConvGRU units. As shown in Figure 2, this also caused two issues of ConvGPPN: scalability to larger maps/iterations (out of memory for 27×27 80 iterations and 49×49 50 and 80 iterations), and also convergence stability (e.g. 27×27 50 iterations).

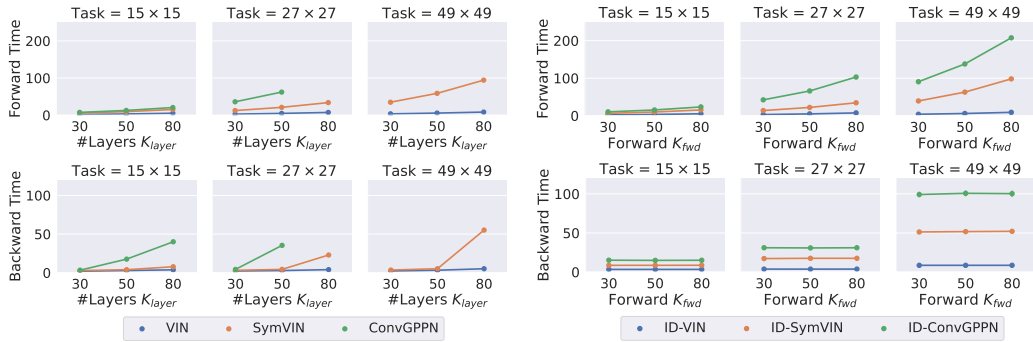


Figure 6: The runtime (in seconds) on 2D navigation tasks with size 15×15 , 27×27 , and 49×49 , averaged over 5 seeds. The explicit planners are on the *left* six figures and the implicit planners on the *right*. *Missing dots* are due to out of memory caused by explicit differentiation. The *upper* row is for forward pass runtime, and the *lower* row is for backward runtime. The horizontal axes mean differently: (1) explicit planners: the number of layers K_{layer} , also number of iterations, and (2) implicit planners: the forward pass iterations K_{fwd} .

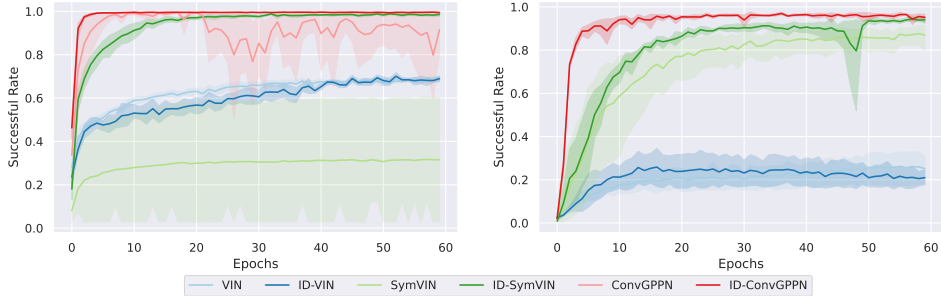


Figure 7: **(Left)** Training curves on 2D maze navigation 15×15 maps, with 80 layers for explicit planners and 80 iterations for implicit planners. **(Right)** Training curves on 49×49 maps, with 30 layers for explicit planners (due to scalability issue) and 80 iterations for implicit planners.

As for SymVIN and ID-SymVIN, they replace Conv2D with SteerableConv, with computational cost slightly higher than VIN and much lower than ConvGPPN. Thus, they can successfully run on all tasks and iteration numbers. However, we find that explicit SymVIN may diverge due to bad initialization, and this is more severe if the network is deeper (more iterations), as in Figure 2’s 50 and 80 iterations. Nevertheless, ID-SymVIN alleviates this issue, since implicit planning decouples forward and backward pass, so the gradient computation is not affected by forward pass.

Furthermore, VIN and ID-VIN are surprisingly less affected by the number of iterations and problem scale. We find their forward passes tends to converge faster to reasonable equilibria, thus further increasing iteration does not help, nor break convergence as long as memory is sufficient.

Forward and backward runtime. We visualize the runtime of explicit and implicit planners in Figure 6. For implicit planners, we use the forward-iteration solver for the forward pass and Anderson solver for the backward pass. Note that in the bottom left, we intentionally plot backward runtime vs. forward pass iterations. This emphasizes that implicit planners decouple forward and backward passes because the backward runtime does not rely on forward pass iterations. Instead, for explicit planners, value iteration is done by network layers, thus the backward pass is coupled: the runtime increases with depth and some runs failed due to limited memory (11GB, see missing dots).

Therefore, this set of figures shows better scalability of implicit planners (no missing dots – out of memory – and constant backward time). In terms of absolute time, the forward runtime of implicit planners when using the *forward solver* is comparable with successful explicit planners.

5.3 TRAINING PERFORMANCE

Setup. Beyond evaluating generalization to novel maps, we compare their training efficiency with learning curves, to give a general impression of the training. Each learning curve is aggregated over 5 seeds, which are from the models in the above section. The learning curves are for all planners on

15×15 maps (Figure 7 left) and 49×49 maps (Figure 7 right, 30 layers for explicit planners – due to scalability issue – and 80 iterations for implicit planners).

Results. On 15×15 maps, we show $K_{\text{layer}} = 80$ layers for explicit planners and $K_{\text{fwd}} = 80$ iterations for implicit planners. ID-ConvGPPN performs the best among all planners and is much more stable than its explicit counterpart ConvGPPN. ID-SymVIN learns reliably, while SymVIN fails to converge due to instability from 80 layers. ID-VIN and VIN are comparable throughout the training. On 49×49 maps, we visualize $K_{\text{layer}} = 30$ layers for explicit planners (due to their limited scalability) and $K_{\text{fwd}} = 80$ iterations for implicit planners. ConvGPPN can not run at all even for only 30 layers, while ID-ConvGPPN still reaches a near-perfect success rate. ID-SymVIN learns slightly better than SymVIN and reaches a better number at the end. ID-VIN has a similar trend to VIN, although it has a slight drop, potentially due to the complexity of the task.

5.4 PERFORMANCE ON MORE TASKS

Table 1: Averaged test success rate (%) over 5 seeds for using 10K/2K/2K dataset on the rest of 3 types of tasks. We highlight entry with *italic* for runs with at least one diverged trial (any success rate < 20%).

Type	Methods	18×18 Mani.	36×36 Mani.	Workspace Mani.	Visual Nav.
Explicit	VIN	89.65 \pm 7.97	74.75 \pm 8.18	80.98 \pm 3.84	66.11 \pm 8.91
	SymVIN	<i>55.15</i> \pm 49.54	<i>65.72</i> \pm 47.11	<i>82.17</i> \pm 24.72	<i>96.04</i> \pm 4.24
	ConvGPPN	79.71 \pm 20.71	70.55 \pm 36.13	70.23 \pm 19.44	81.76 \pm 31.04
Implicit (ours)	ID-VIN	80.53 \pm 6.98	56.27 \pm 20.92	77.17 \pm 7.24	62.53 \pm 15.93
	ID-SymVIN	99.63 \pm 0.08	98.53 \pm 1.42	87.60 \pm 24.11	86.41 \pm 30.34
	ID-ConvGPPN	97.28 \pm 0.74	93.60 \pm 1.68	92.60 \pm 1.83	98.91 \pm 0.34

Setup. We run all planners on the other three challenging tasks. For **visual navigation**, we randomly generate 10K/2K/2K maps using the same strategy as 2D navigation and then render four egocentric panoramic views for each location from produced 3D environments with *Gym-MiniWorld* (Chevalier-Boisvert, 2018). For **configuration-space manipulation** and **workspace manipulation**, we randomly generate 10K/2K/2K tasks with 0 to 5 obstacles in workspace. In configuration-space manipulation, we manually convert each task into a 18×18 or 36×36 map (20° or 10° per bin). The workspace task additionally needs a mapper network to convert the 96×96 workspace (image of obstacles) to an 18×18 2-DOF configuration space (2D occupancy grid). We provide additional details in the Section D.

Results. In Table 1, due to space limitations, we average over $K_{\text{layer}} = 30, 50, 80$ for explicit planners and $K_{\text{fwd}} = 30, 50, 80$ for implicit planners. For each task, we present the mean and standard deviation over 5 seeds times three hyperparameters and delay the separated results to Section E. We italicize entries for runs with at least one diverged trial (any success rate < 20%).

Generally, implicit planners perform much more stably. On 18×18 or 36×36 configuration-space manipulation, ID-SymVIN and ID-ConvGPPN reach almost perfect results, while ID-VIN has diverged runs on 36×36 (marked in *italic*). SymVIN and ConvGPPN are more unstable, while VIN even outperforms them and is also better than ID-VIN. On 18×18 workspace manipulation, because of the difficulty of jointly learning maps and potentially planning on inaccurate maps, most numbers are worse than in configuration-space. ID-ConvGPPN still performs the best, and other methods are comparable. For 15×15 visual navigation, it needs to learn a mapper from panoramic images and is more challenging. ID-ConvGPPN is still the best. ID-SymVIN exhibits some failed runs and gets underperformed by SymVIN in these seeds, and ID-VIN is comparable with VIN.

Across all tasks, the results confirm the superiority of scalability and convergence stability of implicit planners and demonstrate the ability of jointly training mappers (with explicit differentiation for this layer) even when using implicit differentiation for planners.

6 CONCLUSION

This work studies how VIN-based differentiable planners can be improved from an implicit-function perspective: using implicit differentiation to solve the equilibrium imposed by the Bellman equation. We develop a practical pipeline for implicit planning and propose implicit versions of VIN, SymVIN,

and ConvGPPN, which is comparable to or outperforms their explicit counterparts. We find that implicit planners can scale up to longer planning-horizon tasks and larger iterations. In summary, implicit planners are favorable for these cases to explicit planners for several reasons: (1) better performance mainly due to stability, (2) can scale up while some explicit planners fail due to memory limit, (3) less computation time. On the contrary, if using too few iterations, the equilibrium may be poorly solved, and explicit planners should be used instead. While we focus on value iteration, the idea of implicit differentiation is general and applicable beyond path planning, such as in continuous control where Neural ODEs can be deployed to solving ODEs or PDEs.

7 REPRODUCIBILITY STATEMENT

We provide an appendix with extended details of implementation in Section D, experiment details in Section D, and additional results in Section E. We plan to open-source our code next.

REFERENCES

- Brandon Amos and J. Zico Kolter. OptNet: Differentiable Optimization as a Layer in Neural Networks. *arXiv:1703.00443 [cs, math, stat]*, October 2019. URL <http://arxiv.org/abs/1703.00443>. arXiv: 1703.00443.
- Brandon Amos and Denis Yarats. The Differentiable Cross-Entropy Method. September 2019. doi: 10.48550/arXiv.1909.12830. URL <https://arxiv.org/abs/1909.12830v4>.
- Pierre-Luc Bacon, Florian Schäfer, Clement Gehring, Animashree Anandkumar, and Emma Brunskill. A Lagrangian Method for Inverse Problems in Reinforcement Learning. pp. 12, 2019.
- Shaojie Bai, J. Zico Kolter, and Vladlen Koltun. Deep Equilibrium Models. *arXiv:1909.01377 [cs, stat]*, October 2019. URL <http://arxiv.org/abs/1909.01377>. arXiv: 1909.01377.
- Shaojie Bai, Vladlen Koltun, and J. Zico Kolter. Multiscale Deep Equilibrium Models. *arXiv:2006.08656 [cs, stat]*, November 2020. URL <http://arxiv.org/abs/2006.08656>. arXiv: 2006.08656.
- Shaojie Bai, Vladlen Koltun, and J. Zico Kolter. Stabilizing Equilibrium Models by Jacobian Regularization. Technical Report arXiv:2106.14342, arXiv, June 2021. URL <http://arxiv.org/abs/2106.14342>. arXiv:2106.14342 [cs, stat] type: article.
- Devendra Singh Chaplot, Deepak Pathak, and Jitendra Malik. Differentiable Spatial Planning using Transformers. *arXiv:2112.01010 [cs]*, December 2021. URL <http://arxiv.org/abs/2112.01010>. arXiv: 2112.01010.
- Ricky T. Q. Chen, Yulia Rubanova, Jesse Bettencourt, and David Duvenaud. Neural Ordinary Differential Equations. Technical Report arXiv:1806.07366, arXiv, December 2019. URL <http://arxiv.org/abs/1806.07366>. arXiv:1806.07366 [cs, stat] type: article.
- Maxime Chevalier-Boisvert. Miniworld: Minimalistic 3d environment for rl & robotics research. <https://github.com/maximecb/gym-miniworld>, 2018.
- Bruce Christianson. Reverse accumulation and attractive fixed points. *Optimization Methods and Software*, 3(4):311–326, January 1994. ISSN 1055-6788, 1029-4937. doi: 10.1080/10556789408805572. URL <http://www.tandfonline.com/doi/abs/10.1080/10556789408805572>.
- Ignasi Clavera, Violet Fu, and Pieter Abbeel. Model-Augmented Actor-Critic: Backpropagating through Paths. *arXiv:2005.08068 [cs, stat]*, May 2020. URL <http://arxiv.org/abs/2005.08068>. arXiv: 2005.08068.
- Andreea Deac, Petar Veličković, Ognjen Milinković, Pierre-Luc Bacon, Jian Tang, and Mladen Nikoljić. Neural Algorithmic Reasoners are Implicit Planners. October 2021. URL <https://arxiv.org/abs/2110.05442v1>.
- Clement Gehring, Kenji Kawaguchi, Jiaoyang Huang, and Leslie Pack Kaelbling. Understanding End-to-End Model-Based Reinforcement Learning Methods as Implicit Parameterization. May 2021. URL <https://openreview.net/forum?id=xj2sE--Q90e>.
- Laurent El Ghaoui, Fangda Gu, Bertrand Travacca, Armin Askari, and Alicia Y. Tsai. Implicit Deep Learning. Technical Report arXiv:1908.06315, arXiv, August 2020. URL <http://arxiv.org/abs/1908.06315>. arXiv:1908.06315 [cs, math, stat] type: article.
- Jean Charles Gilbert. Automatic differentiation and iterative processes. *Optimization Methods and Software*, 1(1):13–21, January 1992. ISSN 1055-6788. doi: 10.1080/10556789208805503. URL <https://doi.org/10.1080/10556789208805503>. Publisher: Taylor & Francis. eprint: <https://doi.org/10.1080/10556789208805503>.
- Andreas Griewank and Andrea Walther. *Evaluating Derivatives: Principles and Techniques of Algorithmic Differentiation, Second Edition*. SIAM, November 2008. ISBN 978-0-89871-659-7. Google-Books-ID: qMLUIsgCwvUC.

- Christopher Grimm, André Barreto, Satinder Singh, and David Silver. The Value Equivalence Principle for Model-Based Reinforcement Learning. *arXiv:2011.03506 [cs]*, November 2020. URL <http://arxiv.org/abs/2011.03506>. arXiv: 2011.03506.
- Christopher Grimm, André Barreto, Gregory Farquhar, David Silver, and Satinder Singh. Proper Value Equivalence. *arXiv:2106.10316 [cs]*, December 2021. URL <http://arxiv.org/abs/2106.10316>. arXiv: 2106.10316.
- Arthur Guez, Mehdi Mirza, Karol Gregor, Rishabh Kabra, Sébastien Racanière, Théophane Weber, David Raposo, Adam Santoro, Laurent Orseau, Tom Eccles, Greg Wayne, David Silver, and Timothy Lillicrap. An investigation of model-free planning. *arXiv:1901.03559 [cs, stat]*, May 2019. URL <http://arxiv.org/abs/1901.03559>. arXiv: 1901.03559.
- Danijar Hafner, Timothy Lillicrap, Jimmy Ba, and Mohammad Norouzi. Dream to Control: Learning Behaviors by Latent Imagination. *arXiv:1912.01603 [cs]*, March 2020. URL <http://arxiv.org/abs/1912.01603>. arXiv: 1912.01603.
- Kaiming He, Xiangyu Zhang, Shaoqing Ren, and Jian Sun. Deep residual learning for image recognition. *CoRR*, abs/1512.03385, 2015. URL <http://arxiv.org/abs/1512.03385>.
- Peter Karkus, David Hsu, and Wee Sun Lee. QMDP-Net: Deep Learning for Planning under Partial Observability. *arXiv:1703.06692 [cs, stat]*, November 2017. URL <http://arxiv.org/abs/1703.06692>. arXiv: 1703.06692.
- Steven M. LaValle. *Planning Algorithms*. Cambridge University Press, May 2006. ISBN 978-1-139-45517-6.
- Lisa Lee, Emilio Parisotto, Devendra Singh Chaplot, Eric Xing, and Ruslan Salakhutdinov. Gated Path Planning Networks. *arXiv:1806.06408 [cs, stat]*, June 2018. URL <http://arxiv.org/abs/1806.06408>. arXiv: 1806.06408.
- Evgenii Nikishin, Romina Abachi, Rishabh Agarwal, and Pierre-Luc Bacon. Control-Oriented Model-Based Reinforcement Learning with Implicit Differentiation. Technical Report arXiv:2106.03273, arXiv, June 2021. URL <http://arxiv.org/abs/2106.03273>. arXiv:2106.03273 [cs, stat] type: article.
- Sufeng Niu, Siheng Chen, Hanyu Guo, Colin Targonski, Melissa C. Smith, and Jelena Kovačević. Generalized Value Iteration Networks: Life Beyond Lattices. *arXiv:1706.02416 [cs]*, October 2017. URL <http://arxiv.org/abs/1706.02416>. arXiv: 1706.02416.
- Junhyuk Oh, Satinder Singh, and Honglak Lee. Value Prediction Network. *arXiv:1707.03497 [cs]*, November 2017. URL <http://arxiv.org/abs/1707.03497>. arXiv: 1707.03497.
- Vitchyr Pong, Shixiang Gu, Murtaza Dalal, and Sergey Levine. Temporal Difference Models: Model-Free Deep RL for Model-Based Control. *arXiv:1802.09081 [cs]*, February 2018. URL <http://arxiv.org/abs/1802.09081>. arXiv: 1802.09081.
- Olaf Ronneberger, Philipp Fischer, and Thomas Brox. U-net: Convolutional networks for biomedical image segmentation. *CoRR*, abs/1505.04597, 2015. URL <http://arxiv.org/abs/1505.04597>.
- Julian Schrittwieser, Ioannis Antonoglou, Thomas Hubert, Karen Simonyan, Laurent Sifre, Simon Schmitt, Arthur Guez, Edward Lockhart, Demis Hassabis, Thore Graepel, Timothy Lillicrap, and David Silver. Mastering Atari, Go, Chess and Shogi by Planning with a Learned Model. *arXiv:1911.08265 [cs, stat]*, November 2019. URL <http://arxiv.org/abs/1911.08265>. arXiv: 1911.08265.
- Aravind Srinivas, Allan Jabri, Pieter Abbeel, Sergey Levine, and Chelsea Finn. Universal Planning Networks. *arXiv:1804.00645 [cs, stat]*, April 2018. URL <http://arxiv.org/abs/1804.00645>. arXiv: 1804.00645.
- Richard S. Sutton and Andrew G. Barto. *Reinforcement learning: an introduction*. Adaptive computation and machine learning series. The MIT Press, Cambridge, Massachusetts, second edition, 2018. ISBN 978-0-262-03924-6.

- Aviv Tamar, YI WU, Garrett Thomas, Sergey Levine, and Pieter Abbeel. Value Iteration Networks. In *Advances in Neural Information Processing Systems*, volume 29. Curran Associates, Inc., 2016. URL <https://proceedings.neurips.cc/paper/2016/hash/c21002f464c5fc5bee3b98ced83963b8-Abstract.html>.
- Tingwu Wang and Jimmy Ba. Exploring Model-based Planning with Policy Networks. June 2019. URL <https://arxiv.org/abs/1906.08649v1>.
- Théophane Weber, Sébastien Racanière, David P. Reichert, Lars Buesing, Arthur Guez, Danilo Jimenez Rezende, Adria Puigdomènech Badia, Oriol Vinyals, Nicolas Heess, Yujia Li, Razvan Pascanu, Peter Battaglia, Demis Hassabis, David Silver, and Daan Wierstra. Imagination-Augmented Agents for Deep Reinforcement Learning. *arXiv:1707.06203 [cs, stat]*, February 2018. URL <http://arxiv.org/abs/1707.06203>. arXiv: 1707.06203.
- Maurice Weiler and Gabriele Cesa. General $E(2)$ -Equivariant Steerable CNNs. *arXiv:1911.08251 [cs, eess]*, April 2021. URL <http://arxiv.org/abs/1911.08251>. arXiv: 1911.08251.
- Ezra Winston and J. Zico Kolter. Monotone operator equilibrium networks. *arXiv:2006.08591 [cs, stat]*, May 2021. URL <http://arxiv.org/abs/2006.08591>. arXiv: 2006.08591.
- Linfeng Zhao, Xupeng Zhu, Lingzhi Kong, Robin Walters, and Lawson L. S. Wong. Integrating Symmetry into Differentiable Planning. Technical Report arXiv:2206.03674, arXiv, June 2022. URL <http://arxiv.org/abs/2206.03674>. arXiv:2206.03674 [cs] type: article.

CONTENTS

A Outline	14
B Extended Discussion	14
B.1 Computational Similarity	14
C Implementation Details	15
C.1 Implementation of ID-SPT	15
C.2 Optimization of Implicit Planners	15
D Experiment Details	15
D.1 Building Mapper Networks	15
D.2 Training Setup	16
E Additional Results	16
E.1 Generalization to Larger Maps	16
E.2 Runtime of Implicit Planners	17
E.3 Performance on More Tasks: Complete Results	17
E.4 Jacobian Regularization	18

A OUTLINE

We provide additional discussion, extended details of implementation and experiments, and additional results in the appendix. The table of content is available above.

B EXTENDED DISCUSSION

B.1 COMPUTATIONAL SIMILARITY

In value iteration, we iteratively apply f until convergence: $f(v_k, r, \theta) = v_{k+1}$, then the outer loop optimizes one step on updating the model θ . We can generalize to time-varying optimization problem with equality constraint (Bacon et al., 2019): $f_t(v_t, r, \theta_t) = v_{t+1}$, and we assume a mapping ϕ_t gives the inner optimization of VI: $\phi_t = f_{t-1} \circ \dots \circ f_0, \phi_t : \theta_{0:t} \mapsto v_t$. We

$$\frac{\partial \ell}{\partial \theta_t} = \frac{\partial \ell}{\partial v_T} \frac{\partial \phi_T}{\partial \theta_t} = \frac{\partial \ell}{\partial v_T} \lambda_T^\top \quad (7)$$

$$= \frac{\partial \ell}{\partial v_T} \frac{\partial f_{T-1}(v_{T-1}, \theta_{T-1})}{\partial v_{T-1}} \frac{\partial \phi_{T-1}(\theta_{T-1})}{\partial \theta_t} \quad (8)$$

$$= \frac{\partial \ell}{\partial v_T} \frac{\partial f_{T-1}}{\partial v_{T-1}} \frac{\partial f_{T-2}}{\partial v_{T-2}} \dots \frac{\partial \phi_t(\theta_t)}{\partial \theta_t} \quad (9)$$

The recursion is then given by

$$\lambda_T^\top = \frac{\partial \phi_T(\theta_T)}{\partial \theta_T}, \quad \lambda_{k+1}^\top = \frac{\partial f_k}{\partial v_k} \cdot \lambda_k^\top. \quad (10)$$

The vector λ_t^\top is the adjoint vector, or costate, in control theory. The recursive update is the adjoint equation. The computation is exactly the vector-Jacobian product used in automatic differentiation (Griewank & Walther, 2008).

This shows close connection between Equation 6 on the fixed-point solving for backward pass of implicit differentiation and 10 on the recursive computation for explicit differentiation.

C IMPLEMENTATION DETAILS

C.1 IMPLEMENTATION OF ID-SPT

Beyond VIN, SymVIN and ConvGPPN, we also tried implementing an implicit differentiation version of Spatial Planning Transformers (SPT) (Chaplot et al., 2021). However, we find the reimplementation of SPT and also the implicit version both do not work well enough. We first introduce how we implemented it and discuss our hypotheses on its failure.

Implementation. ID-SPT is based on a Transformer architecture, SPT. SPT is proposed to facilitate global value propagation using the global receptive field of self-attention layers in Transformers. Different from other variants, SPT uses heavier global self-attention layer and does not scale up the number of layers with map size, although the number of weights increases quadratically with size. We also implement an implicit version by using individual self-attention layer, where $f(V) = \text{SelfAtt}(V; \theta)$. Even SPT fits into our pipeline, we empirically find SPT behaves unlike other planners since it does not inject reward R as input.

Discussion of performance. In our experiments, we find the modified ID-SPT cannot outperform SPT.

Since SPT uses multiple Transformer (self-attention) layers, it is computationally expensive. Thus, we use much smaller number of iterations for ID-SPT: $K = 3, 5, 10, 15$, because the original paper uses $K = 5$ layers across all map sizes.

However, we plot the convergence curve for its forward and backward pass. We find that the forward pass can only convert to around $10^0 = 1$ to 10^{-1} level (relative residual) and cannot further decrease, while other planners have their forward pass converged around at least 10^{-2} . We find this may affect the backward pass, as the Jacobian at the solved equilibrium is used in solving the backward fixed-point iteration.

Considering these, we think the reason might come from the fact that SPT uses Transformer layers, which is too expressive and tends to learn an arbitrary output as it needs.

C.2 OPTIMIZATION OF IMPLICIT PLANNERS

To optimize the performance of implicit planners, we also implemented other techniques. We tried *Jacobian regularization* from (Bai et al., 2021), which estimates the Jacobian $\left\| \frac{\partial f_{\theta}(\mathbf{v}^*; \mathbf{x})}{\partial \mathbf{v}^*} \right\|_F$ at the equilibrium.

We experiment it on ID-VIN, since other methods have more memory use and Jacobian loss would cause out of memory. However, it does not perform as we expected and rather decreases the success rate. We provide additional results on this in the later result section.

D EXPERIMENT DETAILS

D.1 BUILDING MAPPER NETWORKS

For visual navigation. For navigation, we follow the setting in GPPN (Lee et al., 2018). The input is $m \times m$ panoramic egocentric RGB images in 4 directions of resolution $32 \times 32 \times 3$, which forms a tensor of $m \times m \times 4 \times 32 \times 32 \times 3$. A mapper network converts every image into a 256-dimensional embedding and results in a tensor in shape $m \times m \times 4 \times 256$ and then predicts map layout $m \times m \times 1$.

For the first image encoding part, we use a CNN with the first layer of 32 filters of size 8×8 and stride of 4×4 , and the second layer with 64 filters of size 4×4 and stride of 2×2 , with a final linear layer of size 256.

In the second obstacle prediction part, the first layer has 64 filters and the second layer has 1 filter, all with filter size 3×3 and stride 1×1 .

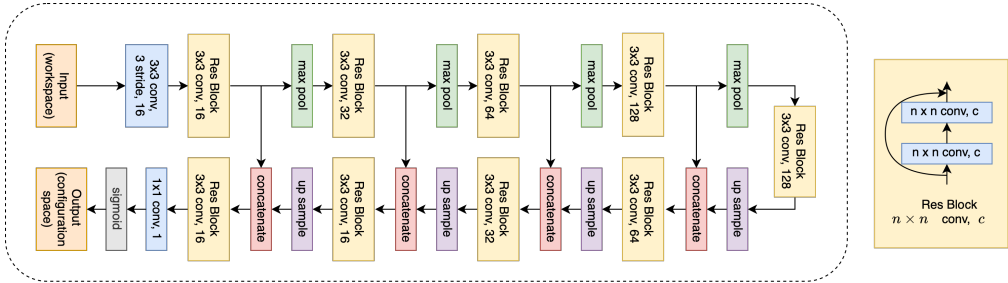


Figure 8: The U-net architecture we used as manipulation mapper.

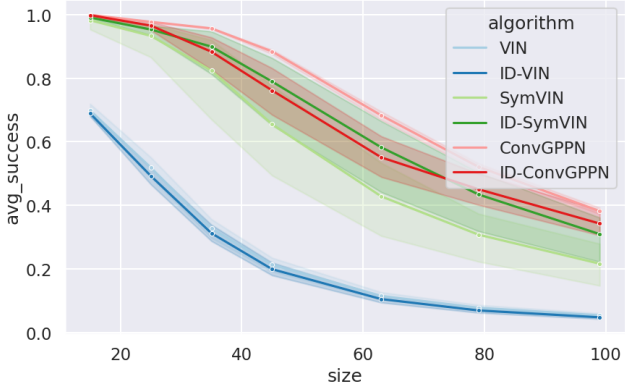


Figure 9: Generalization to larger maps.

For workspace manipulation. For workspace manipulation, we use U-net [Ronneberger et al. \(2015\)](#) with residual-connection [He et al. \(2015\)](#) as a mapper, see Figure.8. The input is 96×96 top-down occupancy grid of the workspace with obstacles, and the target is to output 18×18 configuration space as the maps for planning.

During training, we pre-train the mapper and the planner separately for 15 epochs. Where the mapper takes manipulator workspace and outputs configuration space. The mapper is trained to minimize the binary cross entropy between output and ground truth configurations space. The planner is trained in the same way as described in Section ?? . After pre-training, we switch the input to the planner from ground truth configuration space to the one from the mapper. During testing, we follow the pipeline in [Chaplot et al. \(2021\)](#) that the mapper-planner only have access to the manipulator workspace.

D.2 TRAINING SETUP

We try to mimic the setup in VIN and GPPN ([Lee et al., 2018](#)).

For non-SymPlan related parameters, we use learning rate of 10^{-3} , batch size of 32 if possible (GPPN variants need smaller), RMSprop optimizer.

For SymPlan parameters, we use 150 hidden channels (or 150 *trivial* representations for SymPlan methods) to process the input map. We use 100 hidden channels for Q-value for VIN (or 100 *regular* representations for SymVIN), and use 40 hidden channels for Q-value for GPPN and ConvGPPN (or 40 *regular* representations for SymGPPN on 15×15 , and 20 for larger maps because of memory constraint).

E ADDITIONAL RESULTS

E.1 GENERALIZATION TO LARGER MAPS

Setup. In other experiments, we train the planners on the *same* map size with training case, while this experiment aims for generalization to *larger* maps to examine its potential. All methods are trained on 15×15 maps and tested on larger maps. We chose explicit planners with $K_{layer} = 50$ (for

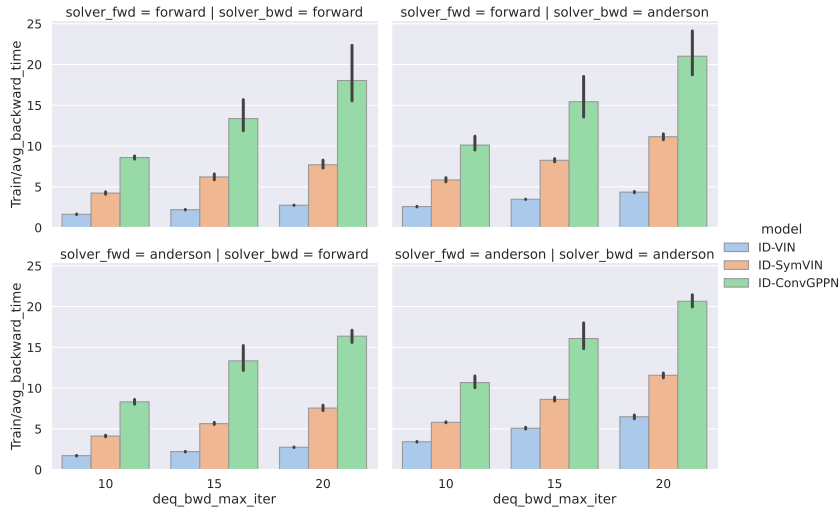


Figure 10: Backward pass iterations vs. backward runtime.

stability concern) and implicit planners with $K_{\text{fwd}} = 80$. All methods are tested on six sampled map sizes in 15×15 through 99×99 , averaging over 5 seeds (5 model checkpoints) for each method and 1000 unseen maps for each map size. At test time, we keep the same iteration numbers as training and do not increase them. The results are shown in Figure 9.

Results. VIN and ID-VIN both suffer from generalizing to larger maps and perform pretty similar. ID-SymVIN is much better than ID-VIN, and outperform the explicit counterpart SymVIN. ID-ConvGPPN generalizes fine, but is worse than ConvGPPN. We find that although ConvGPPN suffers from training on large tasks (backward pass), since here we chose the best hyperparameter for ConvGPPN on 15×15 , its inference (only forward pass) is pretty reliable as long as it can successfully train. As expected, the success rate of all methods drops with increasing test map sizes. While in general, both implicit and explicit planners generalize similarly well. This is expected because implicit differentiation majorly improves scalability of the backward pass, while the main bottleneck for generalization is the forward pass, where they do not have major difference.

E.2 RUNTIME OF IMPLICIT PLANNERS

Backward runtime. We visualize the runtime of **backward pass** of implicit planners for using forward solver and Anderson solver in Figure 10. The experiment is done on 15×15 maps.

As expected, using more backward pass iterations would increase the backward pass runtime. However, we also find that the backward pass has already converged at around 10 iterations, so increasing the iteration will not help the training. Instead, the iterations of the forward pass are the main bottleneck for scalability on larger maps. We show the results in the next paragraph.

Choice of fixed-point solver. We show the performance difference when using different solvers on all implicit differentiable planners in Figure 11. For backward passes, the Anderson solver is clearly better than the forward iteration solver. In terms of the forward passes, ID-SymVIN is not compatible with the original Anderson solver, since SymVIN needs to keep the equivariance of the intermediate variables by ordering them in a specific way. However, the Anderson solver has reshaping operations that would break it.

E.3 PERFORMANCE ON MORE TASKS: COMPLETE RESULTS

In the main paper, we average over 30/50/80 forward iterations / layers. We here show the complete results for each forward iteration / layer number for manipulation in Figure 12 and for visual navigation in Figure 13. The results still follow the trends in the paper, where implicit planners tend to converge more stably for larger iterations.

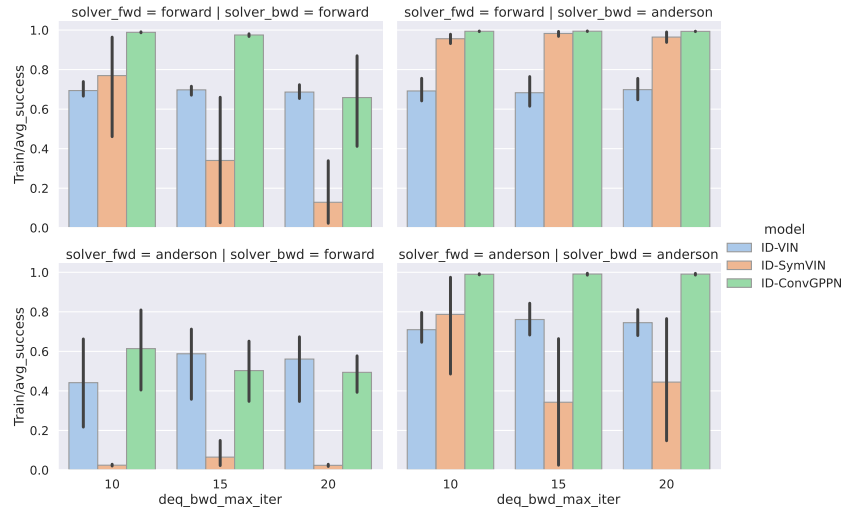


Figure 11: Success rate vs. different forward and backward solver and different backward pass iterations.

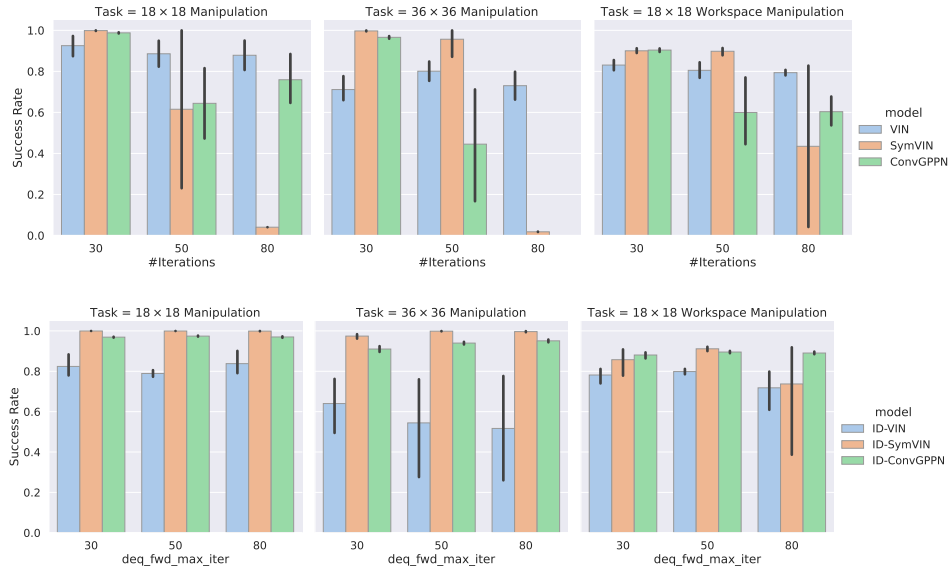


Figure 12: Manipulation complete results.

E.4 JACOBIAN REGULARIZATION

We tune the Jacobian regularization from (Bai et al., 2021). We focus on tuning the Jacobian regularization weight and frequency on 15×15 maps. The x-axis is a hyperparameter of the Anderson solver for backward pass.

The results are in Figure 14. Each column corresponds to the frequency = 0%, 20%, 40%. Each row is the weight = 2, 4, 8. However, the top left panel performs the best, which means zero regularization.

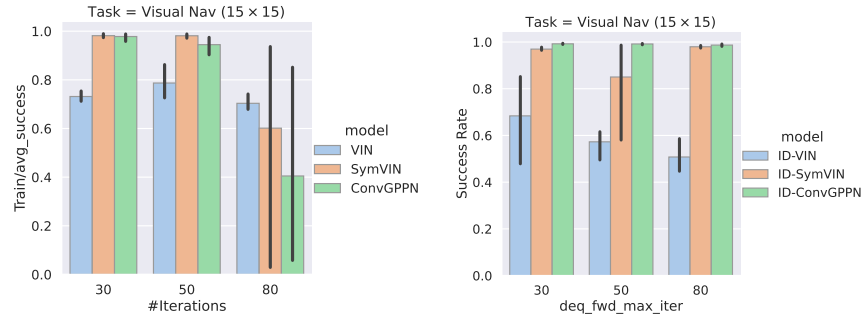


Figure 13: Visual navigation complete results.

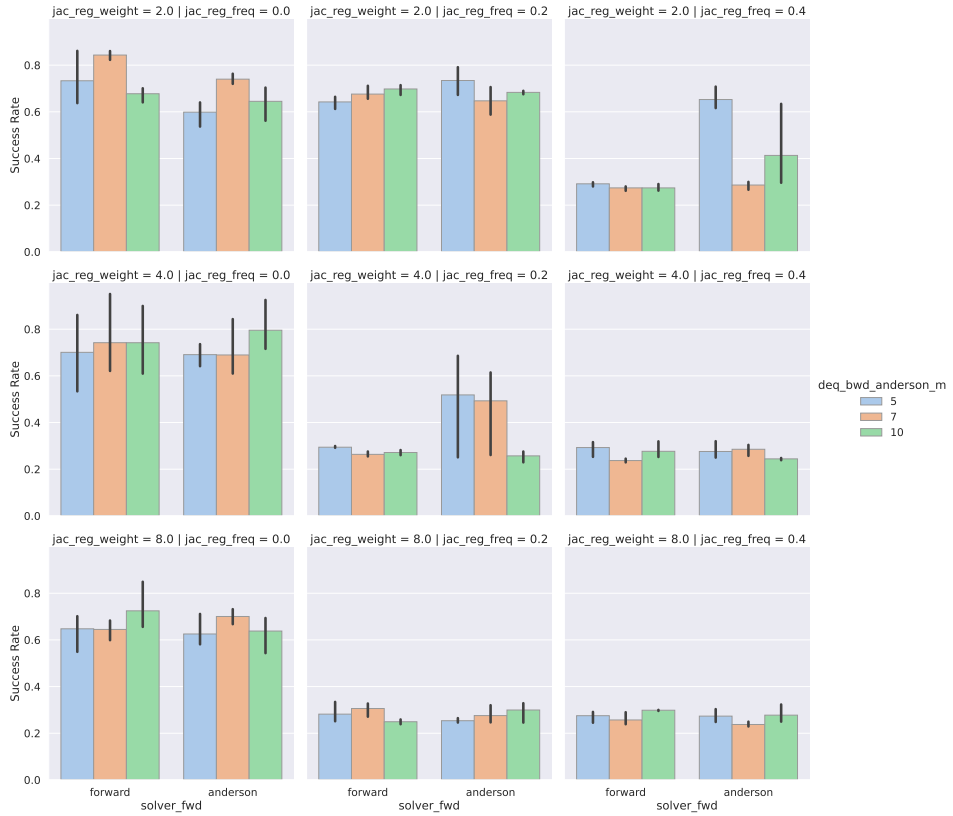


Figure 14: Tuning Jacobian regularization.